

# Quantum Zeno effects from measurement controlled qubit–bath interactions

P. M. Harrington,<sup>1</sup> J. T. Monroe,<sup>1</sup> and K. W. Murch<sup>1,2</sup>

<sup>1</sup>*Department of Physics, Washington University, St. Louis, Missouri 63130*

<sup>2</sup>*Institute for Materials Science and Engineering, St. Louis, Missouri 63130*

(Dated: June 19, 2022)

The Zeno and anti-Zeno effects are features of measurement-driven quantum evolution where frequent measurement inhibits or accelerates the decay of a quantum state. Either type of evolution can emerge depending on the system-environment interaction and measurement method. In this experiment, we use a superconducting qubit to map out both types of Zeno effect in the presence of structured noise baths and variable measurement rates. We observe both the suppression and acceleration of qubit decay as repeated measurements are used to modulate the qubit spectrum causing the qubit to sample different portions of the bath. We compare the Zeno effects arising from dispersive energy measurements and purely-dephasing ‘quasi’-measurements, showing energy measurements are not necessary to accelerate or suppress the decay process.

A projective measurement should reset the clock of a decay process, reinitializing the system to its excited state and therefore inhibiting decay in a variety of situations ranging from nuclear physics [1] to optical lattices [2]. The suppression of a decay process—and more broadly quantum evolution—by frequent measurement is referred to as the “Zeno effect” [3]. The fact that the Zeno effect in decay processes is almost universally negligible is evident by considering Fermi’s golden rule for determining a decay rate: the decay rate depends on the density of states only at the transition frequency and repeated measurement effectively samples a larger range of frequencies. If the bath is Markovian then the larger range samples the same noise and thus the decay rate is unchanged. Therefore, the Zeno effect will only occur under the special circumstance where the density of states is maximum at the transition energy. Rather, the opposite “anti-Zeno effect,” where frequent measurements accelerate decay, is predicted to be a more ubiquitous phenomenon [4–6]. Here we perform a detailed study of both Zeno effects using a superconducting qubit as an emitter coupled to a transmission line with a tunable structured bath. Frequent measurements alter the qubit–bath interaction leading to both accelerated and suppressed decay. Our study expands on the role of measurement in the Zeno effects and highlights new ways to control quantum evolution with tunable bath interactions [7].

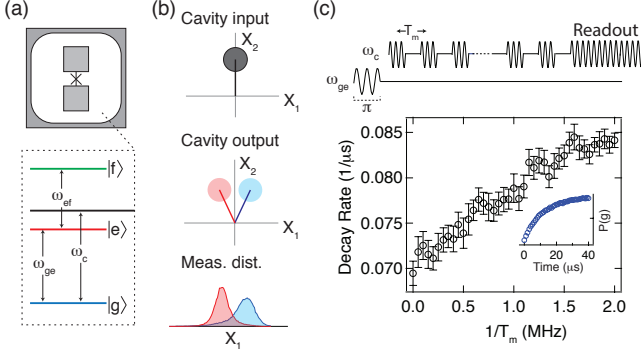
The original development of the Zeno effect predicted the inhibition of particle decay and non-exponential dynamics due to time-evolution interruption from frequent observations [3]. The general case for any quantum system under continuous measurement, dubbed the ‘watchdog-effect’ [8], was explained in terms of cancellation of wavefunction coherence caused from measurement induced perturbations, thus slowing evolution from an initial state [9]. The first experimental measurements of the Zeno effect, conducted with trapped ions [10], incited much discourse on the nature of measurement, the essential features of the Zeno effect, and how the effect compares to simple perturbation dynamics due to ex-

ternal coupling [11, 12]. In recent years, the effect has been generalized as any disruption of the unitary evolution due to projection-like interactions with an external system [13] and it has also been suggested that Zeno-like dynamics can arise from unitary (non-projective) dynamics alone [14–16]. The anti-Zeno effect occurs when frequent measurements accelerate a decay process and was first observed (along with the Zeno effect) in a tunneling experiment with a cold atomic gas [17].

In contrast to previous work [2, 10, 17], our experiment focuses on a single quantum system, where ensemble averaging occurs only after data collection [18]. While the Zeno effect, and more broadly Zeno dynamics, have been studied with superconducting qubits [19–21], the anti-Zeno effect has not yet been studied at the level of a single quantum system. In our experiment, we demonstrate how both Zeno effects arise from frequent projective energy measurements on a superconducting qubit. Furthermore, to examine the role of information in Zeno decay dynamics, we introduce a dephasing-only “measurement” method which does not cause measurement backaction in the energy basis.

Our system consists of a transmon circuit that is dispersively coupled to a three-dimensional waveguide cavity of frequency  $\omega_c/2\pi = 6.895$  GHz (Fig. 1a) [22, 23]. The two lowest energy eigenstates  $\{|g\rangle, |e\rangle\}$  define a qubit with a transition frequency of  $\omega_{ge}/2\pi = 5.103$  GHz. The interaction Hamiltonian,  $H_{\text{int}}/\hbar = -\chi a^\dagger a \sigma_z$  results in a qubit-state-dependent frequency shift of the cavity (Fig. 1b) [24]. Here,  $a^\dagger$  ( $a$ ) is the creation (annihilation) operator for the cavity resonance,  $\sigma_z$  is the Pauli spin operator which has the qubit energy states as an eigenbasis, and  $\chi/2\pi = -1.38$  MHz is the dispersive coupling rate. A probe that populates the cavity with an average intracavity photon number  $\bar{n}$  results in dispersive measurement of the qubit energy state characterized by a timescale  $\tau = \kappa/(16\bar{n}\eta\chi^2)$ , where  $\kappa/2\pi = 6.81$  MHz is the cavity linewidth, and  $\eta = 0.014$  is the measurement quantum efficiency [25–27].

Since the measurement operator  $\sigma_z$  commutes with



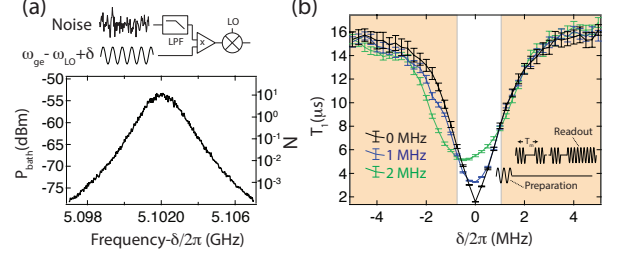
the Hamiltonian, this measurement is considered Quantum Non-Demolition (QND). However, counter-rotating terms and noise-mixing break the QND character of this measurement [28, 29]. To analyze repeated measurements, we perform qubit lifetime measurements while applying 100 ns long probe pulses that occupy the cavity with  $\bar{n} = 9$  intracavity photons. If the probe photons were detected with unity quantum efficiency, then this measurement would distinguish between the energy eigenstates of the circuit with nearly unit fidelity. As such, we consider these measurements to be complete projective measurements, even though the paltry quantum efficiency of the setup inhibits our ability to record these measurements with high fidelity. As shown in Fig. 1c, the observed  $T_1$  of the qubit in the presence of these measurements does decrease, though we emphasize that this alteration of the decay rate is not a Zeno effect as it can easily be explained by considering the non-QND character of the measurement [28, 29].

To study Zeno effects in this system, we introduce a structured thermal bath that alters the decay rate of the transmon circuit. We synthesize a bath of a Lorentzian amplitude spectrum from a white noise source filtered by a low pass  $LC$  filter resulting in a power spectrum with a 3-dB-width of 2 MHz. This low frequency noise is upconverted to near the qubit transition,  $\omega_{ge}$ , via single sideband modulation (Fig. 2b). This thermal photon bath induces stimulated emission and absorption of the qubit, modifying the decay rate. The strength of the bath coupling to the qubit transition is characterized by  $N$ , the average number of thermal photons. Since the bath contributes  $N$  thermal photons, the radiative decay

time decreases as,

$$T_1 = T_{1,\text{spont.}} / (2N + 1) \quad (1)$$

where  $T_{1,\text{spont.}} = 20 \mu\text{s}$  is the radiative decay time from spontaneous emission and  $N$  is the number of thermal photons coupling to the qubit transition [30, 31].



To examine the effect of the synthesized noise bath on the qubit transition decay rate, we perform inversion recovery measurements for different detunings  $\delta$  between the bath-center and the qubit transition. Figure 2b (black line) shows that detuning the center frequency of the bath relative to the qubit transition decreases the  $T_1$  coherence time according to the bath's power spectral density. We note that instead of injecting thermal photons into our system, the electromagnetic spectral density could be colored by the use of a "Purcell filter"—a shunting narrow-band notch filter that suppresses the vacuum fluctuations [32].

We now focus on how repeated measurements alter the coupling of the qubit to a structured thermal environment, thereby reducing or enhancing decay. Figure 2b displays qubit  $T_1$  times versus the bath detuning frequency for different measurement rates. We note that the effect of an increased measurement rate is twofold: the non-QND character of higher measurement rates results in shorter  $T_1$  times (as shown in Fig. 1), and the repeated measurements alter the coupling of the qubit to the synthesized noise bath. To isolate this second effect, we scale the measured  $T_1$  values to eliminate for the non-QND contribution to the measured decay rate, as described in the supplemental information [33].

In comparison to the measured  $T_1$  times in the absence of repeated measurements, the repeated measurements result in regions where the measured  $T_1$  time is decreased (anti-Zeno effect, orange region) and increased (Zeno effect, white region of Fig. 2).

Zeno effects occur because measurement backaction perturbs the system thereby altering its coupling to the bath. The backaction of dispersive  $\sigma_z$  measurements can be understood by considering the interaction Hamiltonian,  $H_{\text{int}}/\hbar = -\chi a^\dagger a \sigma_z$ . On one hand, this interaction describes an ac Stark shift of the qubit transition frequency by intracavity photons. Thus, fluctuations of the intracavity photon number leads to fluctuations of the qubit frequency and thus dephasing. On the other hand, the cavity probe accumulates information about the qubit state in the energy eigenbasis, inducing “spooky” backaction associated with wavefunction collapse [34]. Both the mechanism of photon number fluctuations and the acquired qubit state information perturb the qubit [25, 26, 35], leading to dephasing characterized by a rate  $\Gamma = 8\chi^2\bar{n}/\kappa$  [36, 37]. The presence of these two types of backaction (dephasing versus information accumulation) draws into question the role of information in the Zeno effects. Indeed, a recent proposal [38] has introduced the concept of a “quasi-measurement”—an interaction with the environment that does not necessarily accumulate information about the state—to clarify the role of wavefunction collapse in the Zeno effects.

Accordingly, we implement an alternative measurement scheme which only dephases rather than accumulates information about the qubit state. In the proposal [38], a drive excites the qubit to an auxiliary state which rapidly decays through spontaneous emission (Fig. 3a). This sequence implements a quasi-measurement: if the qubit is in the  $|e\rangle$  state the system will emit a photon, making a projective measurement in the energy basis. Here, we extend this proposal to perform a dephasing-only “measurement,” where no information about the energy state is acquired. To do this, we apply a rotation  $R_{\theta_1}^\pi$  on the  $\omega_{\text{ef}}$  transition to excite the circuit from  $|e\rangle$  to  $|f\rangle$  and then apply a second rotation  $R_{\theta_2}^\pi$  to return the circuit to the  $|e\rangle$  state. These two rotations result in an accumulated Berry phase [39–42] on the state  $|e\rangle$ . To characterize this Berry phase, we perform a Ramsey measurement as shown in Figure 3b. The Ramsey measurements show that the rotations imprint a specific phase evolution on the qubit state related to the phase difference of the two rotations. By randomizing the Berry phase, this interaction completely dephases the qubit state. Furthermore, because the rotations are conducted with a classical drive, no information of qubit’s energy state is acquired in the interaction. These “dephasing measurements” are similar to the dispersive energy measurements, where entanglement between the qubit and environment, and subsequent measurement of the environment, produces a random (owing to the quantum

fluctuation of environment) perturbation on the qubit. For dephasing measurements, however, the perturbation is imprinted on the qubit by the relative phase of the rotations. The quasi-measurements do not acquire information of energy state populations, but instead only dephase the state in the energy eigennbasis.

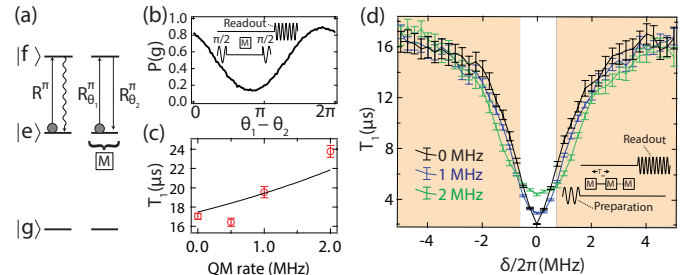


**FIG. 3: Dephasing measurements.** (a) The proposed quasi-measurement from [38] involves excitation to an auxiliary state and spontaneous decay. An alternative, dephasing measurement, uses a second  $\pi$  rotation to return the system to the  $|e\rangle$  state. (b) A Ramsey measurement on the qubit state to characterize the effect of the dephasing measurement. The phase difference of the two rotations in the dephasing measurement imprints Berry phase on the state  $|e\rangle$ . Thus, by randomizing the Berry phase, the interaction dephases the qubit. (c) Measured  $T_1$  times for different measurement rates in the absence of the synthesized noise bath. (d)  $T_1$  decay times in the presence of the synthesized noise bath for different qubit–bath detunings and different measurement rates.

In the experiment, the dephasing measurements are implemented with two Gaussian pulses ( $\sigma = 10$  ns) on the  $\omega_{\text{ef}}$  transition separated by 67 ns. The relative phase between the two pulses is chosen from a pseudo-random number generator. Because each dephasing measurement takes the circuit out of the qubit state manifold, repeated measurements change the effective decay time as shown in Figure 3b, where the solid line indicates the expected dependence on the measured  $T_1$  based on the quasi-measurement rate [33].

We now return to our investigation of the Zeno effects. In Figure 3d, we recreate the  $T_1$  versus detuning data of Figure 2c but have replaced the dispersive  $\sigma_z$  measurements with dephasing quasi-measurements. Here we have our central result: the quasi-measurement scheme exhibits the same decay time pattern as dispersive energy measurements when the bath spectrum is located at specific detunings from the qubit transition. For increasing measurement rates, we find suppressed decay (Zeno-effect, white) when the bath spectrum is near the qubit transition and enhanced decay (anti-Zeno effect, orange) when the bath is further detuned. At higher quasi-measurement rates the Zeno effects become more drastic. Our data show that dephasing measurements induce Zeno effects in a comparable way to projective  $\sigma_z$  measurements.

To probe how the repeated measurements alter the qubit–bath coupling we perform continuous wave spectroscopy of the qubit transition. Accordingly, a weak probe is applied at a variable frequency for a duration of  $80\ \mu\text{s}$  before a projective measurement determines the excited state population. Figure 4 shows how the final excited state population varies as a function of probe frequency for different measurement rates. By increasing measurement rates, we broaden and modulate the qubit transition. Dispersive measurements also result in a slight ac Stark shift of the transition to lower frequencies. The spectroscopy clearly shows how both dispersive and dephasing measurements perturb the qubit transition similarly, such that Zeno effects can arise depending on the spectral properties of the electromagnetic environment.

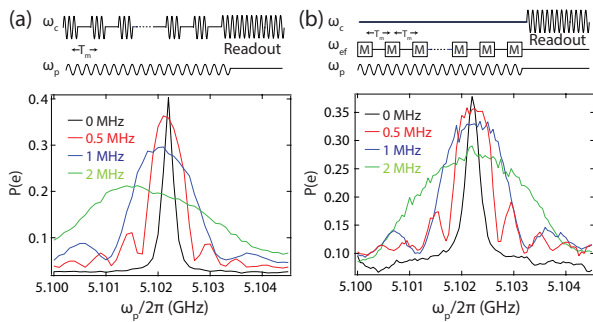


FIG. 4: **Spectroscopy.** A continuous weak probe at frequency  $\omega_p$  is applied for a duration of  $80\ \mu\text{s}$  followed by a projective measurement. The power-broadened qubit transition frequency is revealed as an increase in the final excited state population (black traces). To probe the effects of dispersive (a) and quasi- (b) measurements, we apply these measurements at different measurement rates. (colored curves).

The Zeno and anti-Zeno effects occur from an emitter decoupling from or coupling to its environment. When random measurement perturbations broaden the emitter’s resonance profile, the emitter samples more or less of the bath depending on the spectral density of states. Counter to the original conception of Zeno effects, the measurements that induce broadening of the emitter’s transition do not need to acquire information about the system energy state, but should simply dephase the quantum state.

This experiment demonstrates tools for quantum state engineering through the interplay of radiative decay (dissipative bath interactions), dispersive interactions (projective  $\sigma_z$  measurement), and perturbation by a classical drive (dephasing from quasi-measurement). These methods can be extended to higher dimensional quantum systems to create Zeno dynamics [21, 43–46], where measurement restricts state evolution to certain subspaces.

*Acknowledgements*—We thank N. Tatarsi for early contributions to the experiment, M. Naghiloo and P. Kwiat

for discussions, and D. Tan for sample fabrication. We acknowledge primary research support NSF grant PHY-1607156 and ONR grant No. 12114811. This research used facilities at the Institute of Materials Science and Engineering at Washington University. K.W.M acknowledges support from the Sloan Foundation.

- 
- [1] A. M. Lane, *Physics Letters A* **99**, 359 (1983).
  - [2] Y. S. Patil, S. Chakram, and M. Vengalattore, *Phys. Rev. Lett.* **115**, 140402 (2015).
  - [3] B. Misra and E. C. G. Sudarshan, *J. Math. Phys.* **18**, 756 (1977).
  - [4] B. Kaulakys and V. Gontis, *Phys. Rev. A* **56**, 1131 (1997).
  - [5] A. G. Kofman and G. Kurizki, *Nature* **405**, 546 (2000).
  - [6] P. Facchi, H. Nakazato, and S. Pascazio, *Phys. Rev. Lett.* **86**, 2699 (2001).
  - [7] J. F. Poyatos, J. I. Cirac, and P. Zoller, *Phys. Rev. Lett.* **77**, 4728 (1996).
  - [8] K. Kraus, *Foundations of Physics* **11**, 547 (1981).
  - [9] A. Peres, *Am. J. Phys.* **48**, 931 (198).
  - [10] W. M. Itano, D. J. Heinzen, J. J. Bollinger, and D. J. Wineland, *Phys. Rev. A* **41**, 2295 (1990).
  - [11] L. E. Ballentine, *Phys. Rev. A* **43**, 5165 (1991).
  - [12] W. M. Itano, D. J. Heinzen, J. J. Bollinger, and D. J. Wineland, *Phys. Rev. A* **43**, 5168 (1991).
  - [13] W. M. Itano, arXiv:quant-ph/0612187 (2006).
  - [14] S. Pascazio and M. Namiki, *Phys. Rev. A* **50**, 4582 (1994).
  - [15] L. Viola and S. Lloyd, *Phys. Rev. A* **58**, 2733 (1998).
  - [16] T. Nakanishi, K. Yamane, and M. Kitano, *Phys. Rev. A* **65**, 013404 (2001).
  - [17] M. C. Fischer, B. Gutiérrez-Medina, and M. G. Raizen, *Phys. Rev. Lett.* **87**, 040402 (2001).
  - [18] P. E. Toschek, *EPL* **102**, 20005 (2013).
  - [19] K. Kakuyanag, T. Baba, Y. Matsuzaki, H. Nakano, S. Saito, et al., *New Journal of Physics* **17**, 063035 (2015).
  - [20] D. H. Slichter, C. Müller, R. Vijay, S. J. Weber, A. Blais, et al., *New Journal of Physics* **18**, 053031 (2016).
  - [21] L. Bretheau, P. Campagne-Ibarcq, E. Flurin, F. Mallet, and B. Huard, *Science* **348**, 776 (2015).
  - [22] J. Koch, T. M. Yu, J. Gambetta, A. A. Houck, D. Schuster, et al., *Phys. Rev. A* **76**, 042319 (2007).
  - [23] H. Paik, D. I. Schuster, L. S. Bishop, G. Kirchmair, G. Catelani, et al., *Phys. Rev. Lett.* **107**, 240501 (2011).
  - [24] A. Wallraff, D. I. Schuster, A. Blais, L. Frunzio, M. H. Majer, et al., *Phys. Rev. Lett.* **95**, 060501 (2005).
  - [25] K. W. Murch, S. J. Weber, C. Macklin, and I. Siddiqi, *Nature* **502**, 211 (2013).
  - [26] M. Hatridge, S. Shankar, M. Mirrahimi, F. Schackert, K. Geerlings, T. Brecht, K. M. Sliwa, B. Abdo, L. Frunzio, S. M. Girvin, et al., *Science* **339**, 178 (2013).
  - [27] S. J. Weber, A. Chantasri, J. Dressel, A. N. Jordan, K. W. Murch, et al., *Nature* **511**, 570 (2014).
  - [28] D. H. Slichter, R. Vijay, S. J. Weber, S. Boutin, M. Boissonneault, et al., *Phys. Rev. Lett.* **109**, 153601 (2012).
  - [29] D. Sank, Z. Chen, M. Khezri, J. Kelly, R. Barends, et al., *Phys. Rev. Lett.* **117**, 190503 (2016).
  - [30] C. W. Gardiner, *Phys. Rev. Lett.* **56**, 1917 (1986).
  - [31] K. W. Murch, S. J. Weber, K. M. Beck, E. Ginossar, and

- I. Siddiqi, Nature **499**, 62 (2013).
- [32] M. D. Reed, B. R. Johnson, A. A. Houck, L. DiCarlo, J. M. Chow, et al., Applied Physics Letters **96**, 203110 (2010).
- [33] Further details are given in supplemental information.
- [34] A. N. Korotkov, arXiv:1111.4016 (2011).
- [35] G. de Lange, D. Ristè, M. J. Tiggelman, C. Eichler, L. Tornberg, et al., Phys. Rev. Lett. **112**, 080501 (2014).
- [36] D. I. Schuster, A. Wallraff, A. Blais, L. Frunzio, R.-S. Huang, et al., Phys. Rev. Lett. **94**, 123602 (2005).
- [37] M. Boissonneault, J. M. Gambetta, and A. Blais, Phys. Rev. A **79**, 013819 (2009).
- [38] Q. Ai, D. Xu, S. Yi, A. G. Kofman, C. P. Sun, et al., Scientific Reports **3**, 1752 (2013).
- [39] M. V. Berry, Proc. R.Soc. Lond. **A392**, 45 (1984).
- [40] P. J. Leek, J. M. Fink, A. Blais, R. Bianchetti, M. Göppl, et al., **318**, 1889 (2007).
- [41] A. A. Abdumalikov Jr, J. M. Fink, K. Juliusson, M. Pechal, S. Berger, et al., Nature **496**, 482 (2013).
- [42] C. G. Yale, F. J. Heremans, B. B. Zhou, A. Auer, G. Burkard, et al., Nature Photonics **10**, 184 (2016).
- [43] P. Facchi and S. Pascazio, Phys. Rev. Lett. **89**, 080401 (2002).
- [44] J. M. Raimond, C. Sayrin, S. Gleyzes, I. Dotsenko, M. Brune, et al., Phys. Rev. Lett. **105**, 213601 (2010).
- [45] J. M. Raimond, P. Facchi, B. Peaudecerf, S. Pascazio, C. Sayrin, et al., Phys. Rev. A **86**, 032120 (2012).
- [46] F. Schäfer, I. Herrera, S. Cherukattil, C. Lovecchio, et al., Nat. Commun. **5**, 3194 (2014).

## Supplementary Material

### Inversion Recovery Measurements and Systematic Corrections

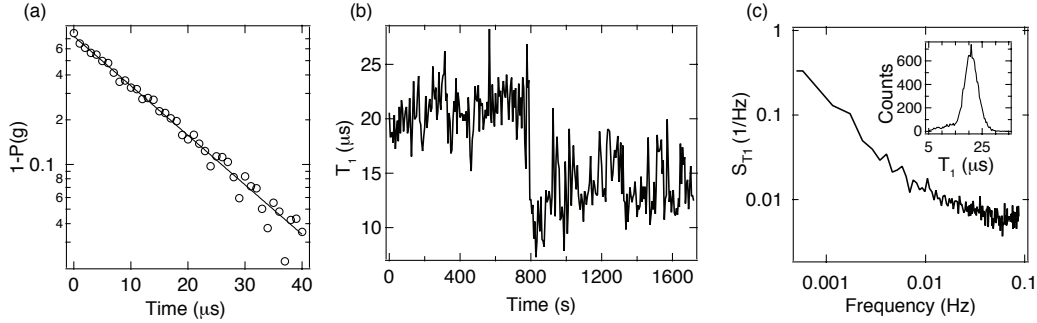


FIG. 5: **Variation in measured  $T_1$  times.** (a) Typical  $T_1$  fit. (b) Variation of  $T_1$  over time. (c) Power spectral density of  $T_1$  fluctuations (inset: histogram of  $T_1$  values obtained over a 24 hour period)

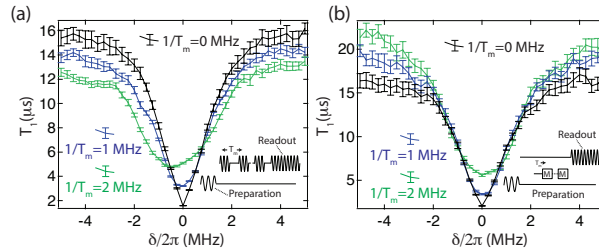


FIG. 6: **Uncorrected  $T_1$  decay curves** (a) Higher dispersive  $z$ -measurement rates uniformly reduce  $T_1$ . (b) Higher quasi-measurement rates tend to increase the measured  $T_1$ .

Figure 5a displays a typical inversion recovery experiment obtained by averaging 2000 measurements at each time point. We fit the rise in ground state population rather than decay of the excited state population to avoid possible effects from coupling to the state  $|f\rangle$ . Figure 5b displays the results of several repeated inversion recovery measurements, showing the presence of long-timescale variations of the  $T_1$  time. The power spectral density of fractional  $T_1$  measurement fluctuations (Fig. 5c) shows that the fluctuations have a  $1/f$  character. Figure 5c (inset) shows a histogram of the measured  $T_1$  values indicating a mean value of  $20 \mu\text{s}$  and significant variance.

The  $T_1$  versus qubit-bath detuning curves at variable measurement rates were collected in the following manner: individual inversion recovery measurements (41 time points, 2000 measurements per point) were collected at each of



41 different qubit–bath detunings for a given measurement rate. These qubit–bath sweep measurements were repeated for different measurement rates. The presented data is composed of the average of 17 qubit–bath sweeps and the error bars indicate the standard error of the mean.

Both the dispersive energy measurements and dephasing measurements that we study in the main text introduce additional systematic effects on the measured  $T_1$  times. In the main text, we present decay curves that are corrected for these systematic effects, and in Figure 6 we display the uncorrected,  $T_1$  measurements indicating that our observed Zeno effects are evident without correction.

The non-QND character of the dispersive energy measurements is described by the dressed-dephasing model of [28], where low-frequency noise in the qubit transition is mixed with cavity photons creating an incoherent drive at the qubit transition. This effect adds an additional decay rate  $\propto \bar{n}$ , which in turn is proportional to the measurement rate. To correct for this effect we use the measured  $T_1$  times for large bath detuning ( $|\delta|/2\pi > 4$  MHz) to determine the additional decay rate arising due to the increased measurement rate and subtract this rate from the measured rates.

The dephasing measurements make use of the auxiliary state  $|f\rangle$  and due to the finite duration of the measurement operation,  $t_m = 100$  ns, each measurement effectively shortens the duration of the inversion recovery experiment due to the system leaving the qubit subspace. This leads to a systematic increase in the apparent  $T_1$  time,  $T_{1,\text{meas.}} = T_1/(1 - t_m/T_m)$ . As shown in Figure 3c, this model roughly accounts for the observed dependence changes in the measured  $T_1$  times. To correct for this effect we use the measured  $T_1$  times for large bath detuning ( $|\delta|/2\pi > 4$  MHz) to determine the linear correction factor for each measurement rate and the  $T_1$  decay curves are scaled accordingly.

### Decay Rate Calculation

The decay rate of an emitter results from coupling of the to environment modes at the transition frequency. The decay rate is calculated by the overlap integral,

$$1/T_1 = 2\pi \int_{-\infty}^{+\infty} d\omega F(\omega, T_m) G(\omega) \quad (2)$$

where  $F(\omega)$  is the qubit transition spectral profile during measurement and  $G(\omega)$  is the environment density-of-states [38]. In our experiment the power spectrum of the thermal noise bath is given by,

$$G(\omega) = \left( \frac{A}{(\omega - \delta)^2 + B^2} \right)^2, \quad (3)$$

where  $\delta$  is the qubit-bath detuning,  $A$  characterizes the strength of the bath, and  $B/2\pi = 1.3$  MHz characterizes the width. Under the approximation that the measurements are instantaneous and projective, qubit transition spectral profile is given by [38],

$$F(\omega, T_m) = T_m \left( \frac{\sin(\omega T_m/2)}{\omega T_m/2} \right)^2. \quad (4)$$

Figure 7 displays the calculated  $T_1$  decay times based on this theory where the only free parameter is the strength of the bath  $A$ . The decay curves exhibit the same qualitative features we see in the experimental data.

### Experimental Apparatus

Figure 8 shows a schematic of the experiment.

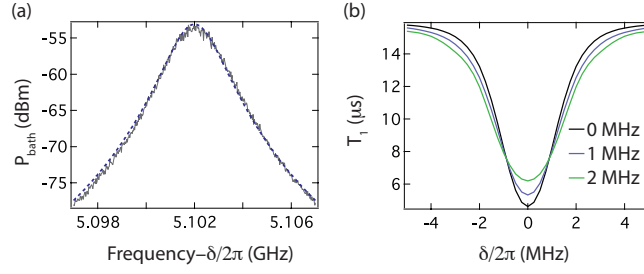


FIG. 7: **Theoretical decay curves** (a) Synthesized thermal bath (gray, solid) and bath model (blue, dashed) given by Eq. (3), (b)  $T_1$  decay times vs qubit-bath detuning calculated using Eq. (2).

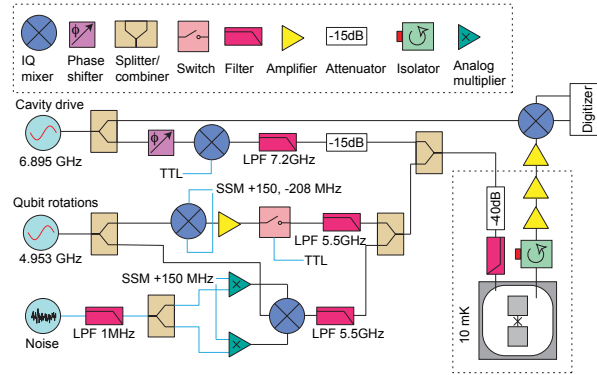


FIG. 8: **Experimental schematic.** State manipulations on the transmon circuit are performed with single sideband modulation. The thermal noise bath is created by mixing low frequency noise up to near the qubit frequency with single sideband modulation.